Engineering Structures 178 (2019) 1–11

Contents lists available at ScienceDirect

Engineering Structures

journal homepage: www.elsevier.com/locate/engstruct

Thermo-mechanical stability analysis of functionally graded shells

M. Rezaiee-Pajand*, D. Pourhekmat, E. Arabi

Department of Civil Engineering, Ferdowsi University of Mashhad, Iran

ARTICLE INFO

Keywords:
Nonlinear analysis
Thermo-mechanical loading
Triangular element
Buckling and post-buckling
Functionally graded materials

ABSTRACT

In this paper, the thermo-elastic nonlinear analysis of various Functionally Graded (FG) shells under different loading conditions is studied. A second-order isoparametric triangular shell element is presented for this purpose. The element is six-noded, and each node has all six independent degrees of freedom in space. It should be added, the first-order shear deformation theory is induced. Furthermore, Voigt's model is adopted to define the FG material properties, which are considered to change gradually from one surface to another. The critical temperature is predicted. Both the pre-buckling and post-buckling equilibrium paths are traced. Since the linear eigenvalue analysis leads to wrong responses in the problems with strong nonlinearity, the suggested procedure is performed based on the FEM and more exact estimations are achieved using equilibrium path.

1. Introduction

Application of composite materials in engineering constructions has a long historical background. From the early usage of straw in mud bricks in masonry structures to the new fiber-matrix laminates applied in aerospace vehicles, all are categorized in the family of composites. Today, nobody has doubts about the advantages of advanced composite materials. Along their widespread usage in industries, the demands for new theories and mathematical modeling capable of predicting their behaviors are increasing rapidly. It is obvious that applying these materials brings some fresh problems that should be considered, as well. For example, laminates show severe stress concentration at the layer interfaces which leads to delamination. Repeated cyclic stresses or impact may cause layers to separate and forming a mica-like configuration of separate layers. As a result, structure can lose significant mechanical toughness. To alleviate this phenomenon, Japanese scientists manufactured a new kind of material, which exhibits a smooth and continues change of material properties through the thickness. This kind of composite was named Functionally Graded (FG) Material.

Until now, many efforts have been made to study the behavior of FG materials [1–3]. Reddy and Chin developed a finite element procedure for FG cylinders and plates, including the thermo-mechanical coupling. They demonstrated the effects of coupling on the temperature distribution, displacements and stresses [4]. Woo and Meguid presented a closed-form solution for large deflection analysis of FG plates and shells. They applied a power law model for material properties' distribution through the thickness. Their solutions were given in Fourier series format [5]. Patel et al. studied geometrically nonlinear responses and thermo-elastic stability characteristics of the cross-ply laminated cylindrical/conical shells with non-circularity/ovality under uniform temperature rise. It should be mentioned, load-displacement curves were obtained with the aid of FEM. They found that the shells with circular cross-section have a distinct bifurcation point, while non-circular ones show a smooth equilibrium path. Furthermore, the effect of initial perturbation/disturbance/imperfection was discussed [6].

Kordkheili and Naghdabadi studied the thermo-elastic behavior of FG plates and shells. They employed the updated Lagrangian framework to carry out nonlinear analysis [7]. By using higher-order shear deformation scheme, Shen performed a thermal post-buckling analysis of FG cylindrical shells. The material properties were considered to be dependent on temperature [8]. Huang and Han extended the large deformation theory of cylindrical shells for buckling and post-buckling analysis of these structures [9]. Alijani et al. took advantages of a multi-modal energy technique and investigated the geometrically nonlinear forced vibration of FG shells. Their research was performed by the analytical approach [10]. Torabi et al. studied the thermal buckling of FG conical shells under thermo-electric loading. In their work, the material properties followed a power law model in thickness direction [11].

Shen and Wang conducted a study on nonlinear bending analysis of FG cylindrical shells resting on elastic foundation. The material properties were assumed to change gradually through the thickness based on Mori-Tanaka scheme [12]. Ghiasian et al. investigated the buckling behavior of FG annular plates in thermal environment. Moreover, Temperature dependency of the material properties was applied in their work. The first-order shear deformation theory was taken into account

* Corresponding author.
E-mail address: rezaiee@um.ac.ir (M. Rezaiee-Pajand).

https://doi.org/10.1016/j.engstruct.2018.09.084
Received 2 April 2018; Received in revised form 18 August 2018; Accepted 28 September 2018
0141-0296/

Nomenclature

a	director vector
$\bar{b}$	body force vector per unit reference volume
$C_{\alpha\beta}$	tangent tensors of elastic moduli
$D_{\alpha\beta}$	stress-strain tensors
d	global deformation vector of element
E	module of elasticity
e_i	orthogonal unit vectors
F	deformation gradient tensor
f	volume fraction
G_α	geometric tensors
h	thickness
I	identity tensor
I_i	strain invariants
J	jacobian
k_α	curvature vectors
k_G	element global tangent stiffness matrix
k_L	element local tangent stiffness matrix
m_α	moment cross-sectional per unit length vectors
$\bar{m}$	external moments per unit reference area
N	interpolation/shape functions matrix
n	power index
n_α	force cross-sectional per unit length vectors
$\bar{n}$	external forces per unit reference area
O	zero tensor
P	first Piola-Kirchhoff stress tensor
P_G	element global secant residual force vector
p_G	global deformation vector of nodes
Q	rotation tensor
$\bar{q}$	generalized external forces vector
R	transformation matrix
r	global effective angles magnitude
T	cauchy stress tensor
$\bar{t}$	surface traction vector per unit reference area
u	global effective displacements vector
x	position vector
z	mapping vector
α	thermal expansion coefficient
γ_α	strain vectors
ΔT	temperature change
$\delta_{\alpha\beta}$	Kronecker delta
δW_{ext}	external virtual work
δW_{int}	internal virtual work
ε_α	strain vectors corresponding to stress-resultant vectors
$\varepsilon_{\alpha\beta}$	permutation symbol
ζ	thickness coordinate
η_α	membrane strain vectors
Θ	global effective angles tensor
θ	global effective angles vector
λ	second Lamé constant
μ	first Lamé constant
ν	Poisson's ratio
ξ_α	surface coordinates
Π	strain energy density function
ρ	arbitrary material property
σ_α	stress-resultant vectors
${}^{th}\sigma_\alpha$	thermal stress-resultant vectors
τ_α	stress vectors
Ψ_α	strain-displacement tensors
Ω	spin tensor
ω	spin vector

to make their formulation capable of modeling thick plates, as well. It should be mentioned that they employed analytical approach [13]. Beheshti and Ramezani studied large deformation analysis of FG shells. They adopted the Enhanced Assumed Strain (EAS) method to mitigate locking problems [14]. Kar and Panda developed a nonlinear model for FG panels to evaluate nonlinear responses of shells subjected to thermo-mechanical loading [15]. In another work, Kar et al. adopted the FEM to investigate the buckling and post-buckling analysis of FG panels under linear and nonlinear thermal gradient loads [16].

Frikha and Dammak presented a shell model for thin and thick panels taking into account finite rotations. They analyzed the effects of material properties on the geometrically nonlinear responses [17]. A closed-form solution for critical load of FG conical shells was proposed by Sofiyev and Kuruoğlu. They used shear deformation theory in conjunction with Galerkin method to reach the governing equations [18]. Moosaie and Panahi-Kalus performed a nonlinear thermo-elastic analysis of FG spherical shells. The material properties were supposed to be dependent on temperature [19]. Rezaiee-Pajand et al. used a six-noded mixed and degenerated triangular shell element for geometrically nonlinear analysis of shells. In their formulation, strain interpolation was applied at the so-called tying points to avoid locking phenomena. Moreover, they solved and compared several popular benchmark examples [20,21]. The parametric thermo-elastic instability of FG cylindrical shell was presented by Li et al. They utilized Hamilton's principle to derive the dynamic governing equations [22].

Prakash et al. investigated the post-buckling behavior of FG skew plates exposed to thermal loading. They employed an eight-noded shear deformable plate bending element. A power-law distribution was used in their work to model the gradually change of material properties in thickness direction [23]. Utilizing finite element method, Abolghasemi et al. studied the buckling of FG plates with elliptical cutout. They applied both mechanical and thermal loading simultaneously and investigated the effect of boundary conditions and cutout radius on FG plates responses [24]. The numerical results of thermo-mechanical buckling of FG plates using isogeometric analysis were presented by Yu et al. These investigators demonstrated the effects of geometric aspects on buckling behavior [25]. Lin et al. developed a refined plate theory for the analysis of FGM circulate panel under thermal and mechanical loads. In this work, they verified their theoretical solutions by comparison with experimental results [26]. Masoodi and Arabi proposed a locking-free shell element for nonlinear analysis of shells exposed to thermo-mechanical loads. Total Lagrangian formulation to taking into account large displacements and rotations was used [27].

The presented review states that all aspects of nonlinear analysis of arbitrary FG shells subjected to thermo-mechanical loading are not covered yet. Based on this fact, the aim of this paper is to present a formulation for predicting the nonlinear responses of various FG shells under thermo-mechanical loads. This study is performed within the framework of FEM. A second-order and six-noded isoparametric triangular shell element is proposed. All six independent degrees of freedom in space for each node are considered. In this research, the Euler-Rodrigues scheme and the first-order shear deformation theory are involved. It should be mentioned, the material properties are expressed via Voigt's model.

2. Material properties distribution

Functionally graded material made of ceramic-metal combination is adopted throughout this study. The properties of this two-phase material are assumed to change gradually from one surface to the other one. Employing the Voigt's model to induce the rule of mixture, material properties are written as a function of the thickness by:

$$\rho(\zeta) = \rho_m f_m(\zeta) + \rho_c f_c(\zeta) \quad (1)$$

Here, ρ demonstrates any material property and f is the volume fraction. The subscripts c and m denote the ceramic and metal. The volume fraction has the following form:

$$
\begin{aligned}
f_m(\zeta) &= 1-f_c \\
f_c(\zeta) &= \left(\frac{\zeta}{h}+\frac{1}{2}\right)^n
\end{aligned} \tag{2}
$$

With substituting Eq. (2) in Eq. (1), one can write:

$$
\rho(\zeta) = \rho_m\left(1-\left(\frac{\zeta}{h}+\frac{1}{2}\right)^n\right)+\rho_c\left(\frac{\zeta}{h}+\frac{1}{2}\right)^n = \rho_m+(\rho_c-\rho_m)\left(\frac{\zeta}{h}+\frac{1}{2}\right)^n \tag{3}
$$

The power index n can take any values between zero and infinity (1000 or higher value), which represents pure-ceramic and pure-metal properties, respectively. Fig. 1 depicts the variation of material properties through the thickness for different values of n. In this paper, $E(\zeta)$, $\nu(\zeta)$ and $\alpha(\zeta)$are module of elasticity, Poisson's ratio and thermal expansion coefficient, respectively. These parameters are function of thickness coordinate and obey the rule of mixture.

3. Kinematical description

In the formulations, tensor notations are utilized. From Greek and Latin indices are also taken benefit, ranging from 1 to 2 and 1 to 3, respectively. Keep in mind, summation convention is adopted over repeated indices. Fig. 2 shows the geometric and kinematic variables besides unit vectors in three configurations used in development of the formulations.

The shell geometry in the reference configuration is given by:

$$
\begin{aligned}
x^r &= z^r + a^r \\
z^r &= \xi_\alpha e^r_\alpha \quad , \quad \xi_1 \in [0\,,\,1] \quad , \quad \xi_2 \in [0,\,1-\xi_1] \\
a^r &= \zeta e^r_3 \quad , \quad \zeta \in [-h/2,\,h/2]
\end{aligned} \tag{4}
$$

In which, h depicts the thickness and $\{\xi_1, \xi_2, \zeta\}$ are the orthogonal unit vectors of reference coordinate. The orthogonal unit vectors in initial configuration are reached, by the subsequent formulas:

$$
\begin{aligned}
e^o_1 &= \frac{z^o_{,1}}{\| z^o_{,1} \|} \\
e^o_2 &= e^o_3 \times e^o_1 \\
e^o_3 &= \frac{z^o_{,1}\times z^o_{,2}}{\| z^o_{,1}\times z^o_{,2} \|}
\end{aligned} \tag{5}
$$

Here, z^oexpress the initial mapping. Note that $(\cdot)_{,\alpha} = \partial(\cdot)/\partial\xi_\alpha$. The initial rotation tensor is written based on the reference and initial unit vectors.

$$
Q^o = e^o_i \otimes e^r_i \tag{6}
$$

The shell director vector in initial configuration is given by:

$$
a^o = Q^o a^r \tag{7}
$$

Then, the geometry of shell in initial space is:

$$
x^o = z^o + a^o \tag{8}
$$

The initial deformation gradient tensor and its back-rotated are in hand by differentiation of x^o with respect to x^r:

$$
\begin{aligned}
F^o &= Q^o F^{or} \\
F^{or} &= I + \gamma^{or}_\alpha \otimes e^r_\alpha
\end{aligned} \tag{9}
$$

In which, I is the identity tensor and initial strain vectors γ^{or}_α have the following definitions:

$$
\begin{aligned}
\gamma^{or}_\alpha &= \eta^{or}_\alpha + k^{or}_\alpha \times a^r \\
\eta^{or}_\alpha &= Q^{oT}\eta^o_\alpha \\
\eta^o_\alpha &= z^o_{,\alpha} - e^o_\alpha \\
k^{or}_\alpha &= Q^{oT}k^o_\alpha \\
k^o_\alpha &= (e^o_3\cdot e^o_{2,\alpha})e^o_1 + (e^o_1\cdot e^o_{3,\alpha})e^o_2 + (e^o_2\cdot e^o_{1,\alpha})e^o_3
\end{aligned} \tag{10}
$$

and:

$$
\begin{aligned}
e^o_{1,\alpha} &= \frac{1}{\| Z^o_{,1} \|}(I - e^o_1 \otimes e^o_1)Z^o_{,1\alpha} \\
e^o_{2,\alpha} &= e^o_3 \times e^o_{1,\alpha} - e^o_1 \times e^o_{3,\alpha} \\
e^o_{3,\alpha} &= \frac{1}{\| Z^o_{,1}\times Z^o_{,2} \|}(I - e^o_3 \otimes e^o_3)(Z^o_{,1}\times Z^o_{,2\alpha} - Z^o_{,2}\times Z^o_{,1\alpha})
\end{aligned} \tag{11}
$$

The effective rotation tensor, based on the Euler–Rodrigues formula, has the following expression [28,29]:

$$
\begin{aligned}
Q^e &= I + h_1\Theta + h_2\Theta^2 \\
h_1 &= \frac{\sin(r)}{r} \quad , \quad h_2 = \frac{1}{2}\left(\frac{\sin(r/2)}{r/2}\right)^2 \\
\Theta &= skew(\theta) \\
r &= \|\theta\| \in (0,\,\pi)
\end{aligned} \tag{12}
$$

where Θ, θ and r are the tensor, vector and magnitude of global effective angles. By means of above relations, the total rotation tensor will be:

$$
Q = Q^e Q^o \tag{13}
$$

The director spin tensor and vector are found as:

$$
\begin{aligned}
\Omega &= skew(\omega) \\
\omega &= \Gamma\delta\theta \\
\Gamma &= I + h_2\Theta + h_3\Theta^2 \\
h_3 &= \frac{1-h_1}{r^2}
\end{aligned} \tag{14}
$$

Here, the symbol δ is used for the incremental values. The shell geometry in the current configuration is as follows:

$$
\begin{aligned}
x &= z + a \\
z &= z^o + u \\
a &= Q a^r
\end{aligned} \tag{15}
$$

In above relations, $u$is the global effective displacements vector. The total gradient of deformation tensor and its back-rotated are calculated by:

$$
\begin{aligned}
F &= Q F^r \\
F^r &= I + \gamma^r_\alpha \otimes e^r_\alpha
\end{aligned} \tag{16}
$$

where total strain vectors γ^r_α have the below relations:

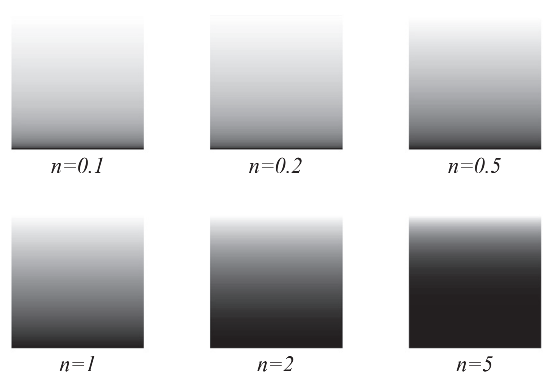

Fig. 1. Variation of material properties through the thickness for different values of n.

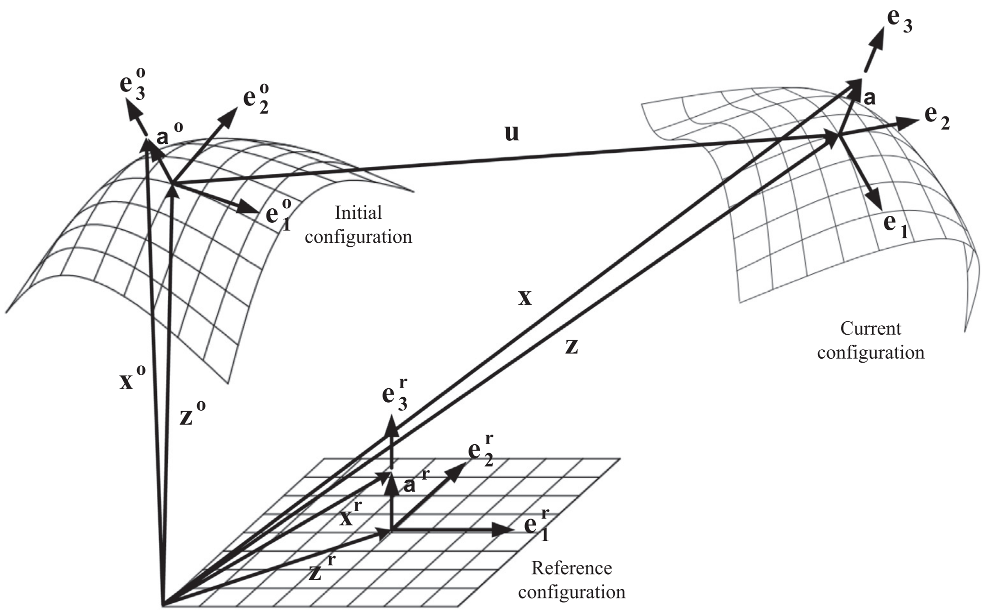

Fig. 2. Geometric and kinematic descriptions.

$$\begin{aligned} \gamma_\alpha^r &= \eta_\alpha^r + k_\alpha^r \times a^r \\ \eta_\alpha^r &= Q^T \eta_\alpha \\ \eta_\alpha &= z_{,\alpha} - e_\alpha \\ k_\alpha^r &= Q^T k_\alpha \\ k_\alpha &= k_\alpha^e + Q^e k_\alpha^o \end{aligned} \tag{17}$$

and:

$$k_\alpha^e = \Gamma \theta_{,\alpha} \tag{18}$$

Now, the effective deformation gradient tensor is obtained using the initial and total ones:

$$F^e = F F^{o-1} \tag{19}$$

By defining of:

$$\begin{aligned} f_\alpha^{or} &= e_\alpha^r + \gamma_\alpha^{or} \\ g_1^{or} &= f_2^{or} \times e_3^r \\ g_2^{or} &= e_3^r \times f_1^{or} \\ f_\alpha^r &= e_\alpha^r + \gamma_\alpha^r \end{aligned} \tag{20}$$

and:

$$f_\alpha^{er} = J^{o-1} (e_\alpha^r \cdot g_\beta^{or}) f_\beta^r \quad , \quad J^o = \det F^o \tag{21}$$

The back-rotated effective strain vectors are given by:

$$\gamma_\alpha^{er} = f_\alpha^{er} - e_\alpha^r \tag{22}$$

Incremental form of the total deformation gradient tensor has the next relation:

$$\begin{aligned} \delta F &= \Omega F + Q(\delta \gamma_\alpha^r \otimes e_\alpha^r) \\ \delta \gamma_\alpha^r &= \delta \eta_\alpha^r + \delta k_\alpha^r \times a^r \\ \delta \eta_\alpha^r &= Q^T (\delta u_{,\alpha} + Z_{,\alpha} \Gamma \delta \theta) \\ \delta k_\alpha^r &= Q^T (\Gamma_{,\alpha} \delta \theta + \Gamma \delta \theta_{,\alpha}) \end{aligned} \tag{23}$$

in which:

$$\begin{aligned} \Gamma_{,\alpha} &= h_2 \Theta_{,\alpha} + h_3 (\Theta \Theta_{,\alpha} + \Theta_{,\alpha} \Theta) + h_4 (\theta \cdot \theta_{,\alpha}) \Theta + h_5 (\theta \cdot \theta_{,\alpha}) \Theta^2 \\ h_4 &= \frac{h_1 - 2h_2}{r^2} \\ h_5 &= \frac{h_2 - 3h_3}{r^2} \\ Z_\alpha &= skew(z_\alpha) \end{aligned} \tag{24}$$

4. Internal and external virtual work

In current configuration, stresses are presented in terms of effective $P^e$and total Pform of the first Piola-Kirchhoff and Cauchy T stress tensor, as follows:

$$\begin{aligned} P^e &= J^e T F^{e-T} \\ J^e &= \det F^e \\ P &= J T F^{-T} \\ J &= \det F = J^e J^o \\ P &= J^o P^e F^{o-T} \end{aligned} \tag{25}$$

P^e and P are expressed with respect to their basic vectors:

$$\begin{aligned} P^e &= \tau^e \otimes e_i^o = Q \tau_i^{er} \otimes e_i^o \\ P &= \tau \otimes e_i^r = Q \tau_i^r \otimes e_i^r \end{aligned} \tag{26}$$

The back-rotated effective and total stress vectors are related to each other by:

$$\tau_\alpha^r = (e_\beta^r \cdot g_\alpha^{or}) \tau_\beta^{er} \tag{27}$$

The internal virtual work per unit volume in the reference coordinate is written as:

$$P: \delta F = J^o P^e : \delta F^e = \tau_\alpha^r \cdot \delta \gamma_\alpha^r = \tau_\alpha^r \cdot \delta \eta_\alpha^r + (a^r \times \tau_\alpha^r) \cdot \delta k_\alpha^r \tag{28}$$

Integrating Eq. (28) through the thickness gives:

$$\int (P: \delta F) d\zeta = n_\alpha^r \cdot \delta \eta_\alpha^r + m_\alpha^r \cdot \delta k_\alpha^r \tag{29}$$

where n_α^r and m_α^r represent forces and moments cross-sectional per unit length of the reference configuration:

$$\begin{aligned} n_\alpha^r &= \int \tau_\alpha^r d\zeta \\ m_\alpha^r &= \int (a^r \times \tau_\alpha^r) d\zeta \end{aligned} \tag{30}$$

By collecting these quantities, the vectors of stress-resultants and corresponding strains are defined:

$$\sigma_\alpha^r = \begin{Bmatrix} n_\alpha^r \\ m_\alpha^r \end{Bmatrix} \quad , \quad \varepsilon_\alpha^r = \begin{Bmatrix} \eta_\alpha^r \\ k_\alpha^r \end{Bmatrix} \tag{31}$$

Then, one can revise Eq. (29) in next form:

$$\int (P: \delta F) d\zeta = \sigma_\alpha^r \cdot \delta \varepsilon_\alpha^r \tag{32}$$

The relation between incremental strains and deformations, with the aid of strain-deformation tensors, is as follows:

$$\delta\varepsilon_\alpha^r = \Psi_\alpha \delta d$$
$$\Psi_\alpha = \begin{bmatrix} Q^T & O \\ O & Q^T \end{bmatrix}\begin{bmatrix} I & O & Z_{,\alpha}\Gamma \\ O & \Gamma & \Gamma_{,\alpha} \end{bmatrix}\Delta_\alpha$$
$$\Delta_\alpha = \begin{bmatrix} I\frac{\partial}{\partial\xi_\alpha} & O \\ O & I\frac{\partial}{\partial\xi_\alpha} \\ O & I \end{bmatrix}$$
$$d = \begin{Bmatrix} u \\ \theta \end{Bmatrix} \tag{33}$$

Here, O is the zero tensor. The shell internal virtual work is:

$$\delta W_{int} = \iiint (P\colon \delta F)\, d\zeta d\xi_1 d\xi_2 = \iint (\sigma_\alpha^r \cdot \delta\varepsilon_\alpha^r)\, d\xi_1 d\xi_2 \tag{34}$$

If $\bar{t}^t$and $\bar{t}^b$present the traction force vectors of the top and bottom surfaces per unit reference area, respectively, and $\bar{b}$ depicts the body force vector per unit reference volume; the external virtual work of the shell will be:

$$\delta W_{ext} = \iint [\bar{t}^t\cdot\delta x^t + \bar{t}^b\cdot\delta x^b + \int (\bar{b}\cdot\delta x)\, d\zeta]\, d\xi_1 d\xi_2 \tag{35}$$

$\dot{x}$ by time differentiation of x is available:

$$\delta x = \delta u + \omega \times a \tag{36}$$

External forces and moments per unit reference area, can be shown in subsequent vectors:

$$\bar{n} = \bar{t}^t + \bar{t}^b + \int \bar{b}\, d\zeta$$
$$\bar{m} = a^t \times \bar{t}^t + a^b \times \bar{t}^b + \int (a \times \bar{b})\, d\zeta \tag{37}$$

For compaction, the vector of generalized external forces is introduced:

$$\bar{q} = \begin{Bmatrix} \bar{n} \\ \Gamma^T \bar{m} \end{Bmatrix} \tag{38}$$

The external virtual work per unit reference volume in Eq. (35) is rewritten as:

$$\delta W_{ext} = \iint (\bar{q}\cdot\delta d)\, d\xi_1 d\xi_2 \tag{39}$$

By employing the principle of virtual work, along with the usage of Eqs. (34) and (39), the next relation is held:

$$\delta W = \delta W_{int} - \delta W_{ext} = 0 \;\Rightarrow\; \iint (\sigma_\alpha^r\cdot\delta\varepsilon^r)\, d\xi_1 d\xi_2 - \iint (\bar{q}\cdot\delta d)\, d\xi_1 d\xi_2 = 0 \tag{40}$$

Expressions of σ_α^r, $\delta\varepsilon^r$, $\bar{q}$ andδd, which are given in Eqs. (31), (33) and (38), are substituted into Eq. (40). Subsequently, the integration by parts is performed. After collecting the coefficients of δu and $(\Gamma\delta\theta)$ separately and setting them to zero, the following local equilibrium equations are reached:

$$n_{\alpha,\alpha} + \bar{n} = 0$$
$$m_{\alpha,\alpha} + z_{,\alpha} \times n_\alpha + \bar{m} = 0 \tag{41}$$

where

$$n_\alpha = Q n_\alpha^r, \quad m_\alpha = Q m_\alpha^r \tag{42}$$

On the other hand, by some substitutions and calculations and also assuming the locally conservation of external load, Eq. (40) lead to the next tangent bilinear expression:

$$\delta W = \iint [(\Psi_\alpha \delta d)\cdot(D_{\alpha\beta}\Psi_\beta d) + (\Delta_\alpha \delta d)\cdot(G_\alpha \Delta_\alpha d)]\, d\xi_1 d\xi_2 \tag{43}$$

with:

$$D_{\alpha\beta} = \frac{\partial\sigma_\alpha^r}{\partial\varepsilon_\beta^r} = \begin{bmatrix} \frac{\partial n_\alpha^r}{\partial\eta_\beta^r} & \frac{\partial n_\alpha^r}{\partial k_\beta^r} \\ \frac{\partial m_\alpha^r}{\partial\eta_\beta^r} & \frac{\partial m_\alpha^r}{\partial k_\beta^r} \end{bmatrix}$$
$$G_\alpha = \begin{bmatrix} O & O & G_\alpha^{u'\theta} \\ O & O & G_\alpha^{\theta'\theta} \\ G_\alpha^{\theta u'} & G_\alpha^{\theta\theta'} & G_\alpha^{\theta\theta} \end{bmatrix} \tag{44}$$

The sub-matrices of geometric tensors G_α are reported in [30,31].

5. Plane-stress state

It should be noted, the plane-stress condition is applied.

$$f_3^r = f_3^{er} = (1 + \gamma_{33}) e_3^r \tag{45}$$

where γ_{33} is the strain in thickness direction. Keeping in mind that although γ_{33} is nonzero, but based on the plane-stress assumption, the corresponding stress will be zero. In other words:

$$\tau_{33}^r = \tau_{33}^{er} = 0 \tag{46}$$

Therefore, the energy due to this strain is vanished.

6. Isotropic elastic material

Defining $\Pi(I_1^e, I_2^e, I_3^e)$ as the strain energy function per unit initial volume for isotropic elastic material while I_1^e, I_2^e, and I_3^e are strain invariants, the following descriptions are available:

$$I_1^e = J^e = \det F^e$$
$$I_2^e = F^e\colon F^e$$
$$I_3^e = \tfrac{1}{2}(F^{eT}F^e)\colon (F^{eT}F^e) \tag{47}$$

Using the hyperelastic neo-Hookean-type material model, strain energy density function and its strain invariants have the form of [32]:

$$\Pi(I_1^e, I_2^e) = \tfrac{1}{2}\lambda[\tfrac{1}{2}(I_1^{e2} - 1) - \ln I_1^e] + \tfrac{1}{2}\mu(I_2^e - 2\ln I_1^e - 3)$$
$$I_1^e = J^e = (1 + \gamma_{33})\bar{J}^e$$
$$\bar{J}^e = (1 + e_\alpha^r\cdot\gamma_\alpha^{er} + e_3^r\cdot\gamma_1^{er} \times \gamma_2^{er})$$
$$I_2^e = F^e\colon F^e = 3 + 2e_i^r\cdot\gamma_i^{er} + \gamma_i^{er}\cdot\gamma_i^{er} \tag{48}$$

The back-rotated effective stress vectors are stated as:

$$\tau_\alpha^{er} = \frac{\partial\Pi}{\partial\gamma_\alpha^{er}} = \frac{\partial\Pi}{\partial I_\beta^e}\frac{\partial I_\beta^e}{\partial\gamma_\alpha^{er}} = [\frac{1}{2}\lambda(J^{e2} - 1) - \mu]\frac{1}{\bar{J}^e} g_\alpha^{er} + \mu f_\alpha^{er} \tag{49}$$

In above equations, μ and λ are Lamé constants, and the next relations are established:

$$\mu = \frac{E}{2(1 + \nu)}$$
$$\lambda = \frac{E\nu}{(1 + \nu)(1 - 2\nu)} \tag{50}$$

also:

$$g_\alpha^{er} = \varepsilon_{\alpha\beta} f_\beta^{er} \times e_3^r \tag{51}$$

by defining the below quantities:

$$\varphi(\bar{J}^e) = -\mu\frac{\lambda + 2\mu}{\lambda\bar{J}^{e3} + 2\mu\bar{J}^e}$$
$$\varphi'(\bar{J}^e) = \frac{\partial\varphi}{\partial\bar{J}^e} = \mu\frac{(\lambda + 2\mu)(3\lambda\bar{J}^{e2} + 2\mu)}{(\lambda\bar{J}^{e3} + 2\mu\bar{J}^e)^2} = -\varphi(\bar{J}^e)\frac{3\lambda\bar{J}^{e2} + 2\mu}{\lambda\bar{J}^{e3} + 2\mu\bar{J}^e} \tag{52}$$

Eq. (51) leads to:

$$\tau_\alpha^{er} = [\mu + \varphi(\bar{J}^e)]e_\alpha^r - \varepsilon_{\alpha\beta}\varphi(\bar{J}^e)(e_3^r \times \gamma_\beta^{er}) + \mu\gamma_\alpha^{er} \tag{53}$$

The back-rotated total and effective tangent tensors of elastic moduli are introduced as:

$$C^r_{\alpha\beta} = \frac{\partial\tau^r_\alpha}{\partial\gamma^r_\beta} = J^{o-1}(e^r_\gamma \cdot g^{or}_\alpha)(e^r_\delta \cdot g^{or}_\beta)C^{er}_{\gamma\delta}$$
$$C^{er}_{\alpha\beta} = \frac{\partial\tau^{er}_\alpha}{\partial\gamma^{er}_\beta} = \varphi'(\bar{J}^e)g^{er}_\beta + \delta_{\alpha\beta}\mu I - \varepsilon_{\alpha\beta}\varphi(\bar{J}^e)E^r_3 \tag{54}$$

in which:

$$E^r_3 = skew(e^r_3) \tag{55}$$

It should be noticed that $\delta_{\alpha\beta}$ is the Kronecker delta and $\varepsilon_{\alpha\beta}$ shows the permutation symbol. It means:

$$\delta_{11} = 1,\quad \delta_{12} = 0,\quad \delta_{21} = 0,\quad \delta_{22} = 1$$
$$\varepsilon_{11} = 0,\quad \varepsilon_{12} = 1,\quad \varepsilon_{21} = -1,\quad \varepsilon_{22} = 0 \tag{56}$$

Finally, the sub-matrices of stress-strain tensors $D_{\alpha\beta}$ are in hand:

$$\frac{\partial n^r_\alpha}{\partial \eta^r_\beta} = \int C^r_{\alpha\beta}\, d\zeta,\quad \frac{\partial n^r_\alpha}{\partial k^r_\beta} = -\int C^r_{\alpha\beta}A^r\, d\zeta$$
$$\frac{\partial m^r_\alpha}{\partial \eta^r_\beta} = \int A^r C^r_{\alpha\beta}\, d\zeta,\quad \frac{\partial m^r_\alpha}{\partial k^r_\beta} = -\int A^r C^r_{\alpha\beta}A^r\, d\zeta \tag{57}$$

where

$$A^r = skew(a^r) \tag{58}$$

7. Finite element discretization

In this study, a second-order isoparametric triangular shell element is introduced. The element is six-noded, and as depicted in Fig. 3, all six independent degrees of freedom are assigned per node. The element shape functions for each node are given by:

$$N_1 = \xi_3(2\xi_3 - 1),\quad N_2 = \xi_1(2\xi_1 - 1),\quad N_3 = \xi_2(2\xi_2 - 1)$$
$$N_4 = 4\xi_3\xi_1,\quad N_5 = 4\xi_1\xi_2,\quad N_6 = 4\xi_2\xi_3 \tag{59}$$

If N is the matrix of interpolation functions due to element, the relation between nodal p_G and elemental d global deformations will be:

$$d = Np_G \tag{60}$$

Based on Eq. (40), the global vector of the element secant residual force is computed as:

$$P_G = \iint [N^T\bar{q} - (\Psi_\alpha N)^T\sigma^r_\alpha - (\Psi_\alpha N)^T\, {}^{th}\sigma^r_\alpha]\, d\xi_1 d\xi_2 \tag{61}$$

Superscript th indicates to thermal components. By taking advantage of Eq. (43), the global tangent stiffness matrix of the element is also obtained:

$$k_G = \iint [(\Psi_\alpha N)^T D_{\alpha\beta}(\Psi_\beta N) + (\Delta_\alpha N)^T G_\alpha(\Delta_\alpha N)]\, d\xi_1 d\xi_2 \tag{62}$$

Note, the corresponding components to the drilling degrees of freedom in the element local stiffness matrix is added with an artificial stiffness of Eh^3 [33,34]. The transformation matrix needed for this action, has the form of:

$$R = \begin{bmatrix} Q & & & & & & & & & & & \\ & Q & & & & & & & & & & \\ & & Q & & & & & & O & & & \\ & & & Q & & & & & & & & \\ & & & & Q & & & & & & & \\ & & & & & Q & & & & & & \\ & & & & & & Q & & & & & \\ & & & & & & & Q & & & & \\ & & & & & & & & Q & & & \\ & & O & & & & & & & Q & & \\ & & & & & & & & & & Q & \\ & & & & & & & & & & & Q \end{bmatrix} \tag{63}$$

According to the common rule, the relation between local and global element stiffness matrices is written by:

$$k_L = R^T k_G R$$
$$k_G = R k_L R^T \tag{64}$$

8. Numerical studies

Based on the aforementioned formulations, a code is written in FORTRAN language. It is worth mentioning, three in-plane within nine through-the-thickness Gauss integration points are used for the element stiffness matrix and residual force vector computations. In this study, the governing nonlinear equations are solved by using the Generalized Displacement Control Method (GDCM) [20]. The numerical studies are briefly stated in the following lines. Solving the first two problems is aimed to validate and versatile the present formulation via comparison with the others published literature. The last two shells are designed and reported to show the capability of authors' method in analysis of FG shells. Moreover, they can be utilized as benchmark problems for the future studies. Keeping in mind that in the following first two problems, the lower and upper surfaces, and in the next two problems, the inner and outer surfaces, are metal-rich and ceramic-rich, respectively.

8.1. Shallow cylindrical panel

Fig. 4 shows a shallow cylindrical shell subjected to a point load. As it is seen, only one-fourth of the shell is discretized due to symmetry. The material data are:

Zirconium Oxide (ZrO_2): $E_c = 151 \times 10^3\, N/mm^2$, $\upsilon_c = 0.3$
Aluminium (Al) : $E_m = 70 \times 10^3\, N/mm^2$, $\upsilon_m = 0.3$

At first, a convergence study is performed with different mesh of $2 \times 2 \times 2$, $2 \times 4 \times 4$, $2 \times 8 \times 8$ and $2 \times 16 \times 16$ elements. The power index is assumed to be $n = 1$. The shell thickness is 12.7 mm. The results for deflection at the point load are inserted in Table 1.

Based on the aforementioned convergence study, the mesh pattern of $2 \times 8 \times 8$ is employed for further investigation. The cases considered are thickness of 6.35 mm and 12.7 mm with the maximum point load of $P = 2 \times 10^5 N$ and $P = 4 \times 10^5 N$, respectively. It should be noted that the panel is hinged at the straight edges and free at curved ones.

The load-deflection curves of this structure for the point under the load are depicted in Fig. 5. Moreover, the results reported by Arciniega and Reddy [35] are also given for the comparison purpose. According to the obtained outcomes, excellent agreement is observed between the results.

8.2. Thermal buckling of annular plate

Buckling of annular plate is analyzed under uniform heat $\Delta T = 1400$ K. The material properties used in this study are:

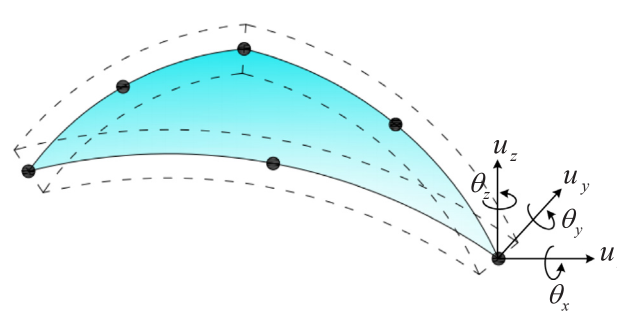

Fig. 3. Six-noded triangular shell element and nodal degrees of freedom.

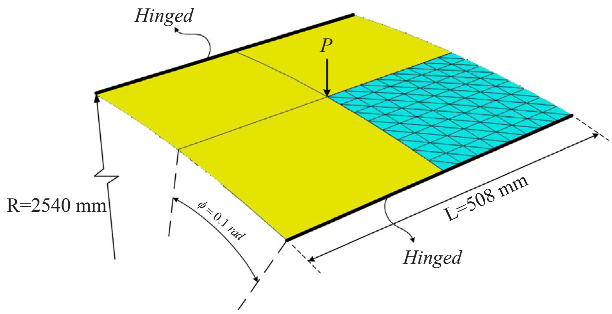

Fig. 4. Shallow cylindrical shell under point load.

Table 1
Convergence study for shallow panel.

Mesh pattern	2 × 2 × 2	2 × 4 × 4	2 × 8 × 8	2 × 16 × 16
Deflection (mm)	39.81	40.57	40.84	40.88
Error (%)	2.62	0.76	0.10	0.00

Silicon Nitride (Si_3N_4): $E_c = 322 \times 10^5 N/cm^2$, $\alpha_c = 7.5 \times 10^{-6} K^{-1}$, $\nu_c = 0.3$

Stainless Steel $(SS304)$: $E_m = 208 \times 10^5 N/cm^2$, $\alpha_m = 15.3 \times 10^{-6} K^{-1}$, $\nu_m = 0.3$

Two parameters are introduced in the following line:

$\delta = thickness\,(h)/outer\ radius\,(R_o)$, $\beta = inner\ radius\,(R_i)\,/outer\ radius\,(R_o)$

It should be noted that the mesh pattern used for the half of the plate is $2 \times 4 \times 20$ and $2 \times 14 \times 20$ for $\beta = 0.6$ and $\beta = 0.1$, respectively. Fig. 6 shows this model discretization.

In the case (I), the analysis is performed for different values of β. Other geometric data are:

$R_o = 100\,\text{cm}$, $\delta = 0.03$

For the case (II), the critical thermal buckling load is evaluated with different amounts of δ. The geometry characteristics are as follows:

$R_o = 100\,\text{cm}$, $\beta = 0.5$

Verification of the formulation is demonstrated via comparison with the analytical results reported by Ghiasian et al. [13] in Table 2. Note, the solutions are corresponded to $n = 1$ and the tabulated data are picked from the graphs.

As it is seen, the results are very close. In Fig. 7, the load-deflection curves for point A of cases (I) and (II), are given for different values of β and δ, respectively. It is worth mentioning that two out of plane disturbance point loads 100 N are used.

Responses show that the thermal buckling load increases as the values of β and δ become higher. This is because raising the values of δ and β results in stiffer structure since both inner and outer edges are clamped.

8.3. Cylindrical shell

Fig. 8 exhibits a cylindrical shell with fixed ends subjected to the thermal, mechanical and thermo-mechanical loading. The geometric data are $R = 100\,\text{cm}$, $L = 100\,\text{cm}$ and $h = 1\,\text{cm}$, denoting radius, length and thickness of the shell, respectively. Next values are the shell material properties:

Aluminium Oxide (Al_2O_3): $E_c = 380 \times 10^5\,\text{N/cm}^2$, $\alpha_c = 7.4 \times 10^{-6}\,\text{K}^{-1}$, $\nu_c = 0.3$

Nickel (Ni) : $E_m = 205 \times 10^5\,\text{N/cm}^2$, $\alpha_m = 12.5 \times 10^{-6}\,\text{K}^{-1}$, $\nu_m = 0.3$

Three cases are considered for this problem. At first, thermal buckling and post-buckling behavior of the shell is investigated in the thermal environment of $\Delta T = 2000\,\text{K}$. In order to trace the post-buckling equilibrium path, two opposite outward diametrical point loads with the value of $4000\,N$ are applied as perturbation loads. The responses are obtained at point A and reported in Fig. 9(a). Secondly, this structure is studied under outward pressure load of $p = 50000\,\text{N/cm}^2$. The load-displacement curves of point A are depicted in Fig. 9(b). Last but not least, the nonlinear analysis of cylindrical shell is carried out under thermo-mechanical loading. Thermal change is $\Delta T = 2000\,K$ and the applied pressure load of $p = 50000\,\text{N/cm}^2$ is assumed. The obtained results are given for point A in Fig. 9(c). It is worth mentioning, a mesh of $2 \times 16 \times 48$ triangular shell element is used to model one octant of the structure. As it is predicted, the thermal loading effects on responses rise when n grows. In other words, as the volume fraction index n increases, the thermal buckling occurs at the lower temperature levels, which arises from the fact that by increasing n, the material properties and thermal coefficient close to fully metal behavior.

8.4. Conical shell

In this example, the behavior of a truncated conical shell is investigated. As it is shown in Fig. 10, the shell is clamped at both edges.

The geometric characteristics are inserted in Table 3.

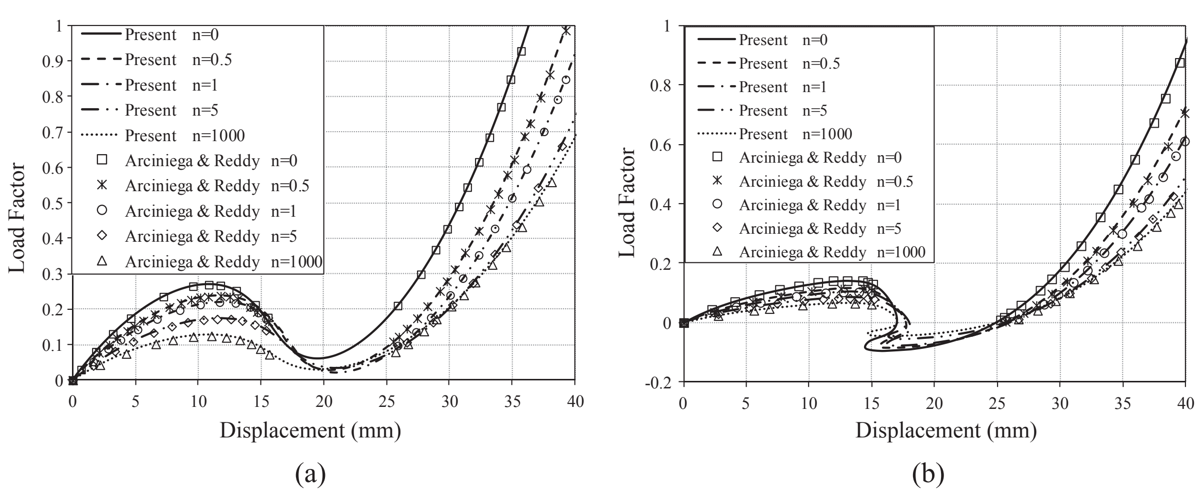

Fig. 5. Load-deflection curves of shallow panel, (a) Thickness of 12.7 mm, (b) Thickness of 6.35 mm.

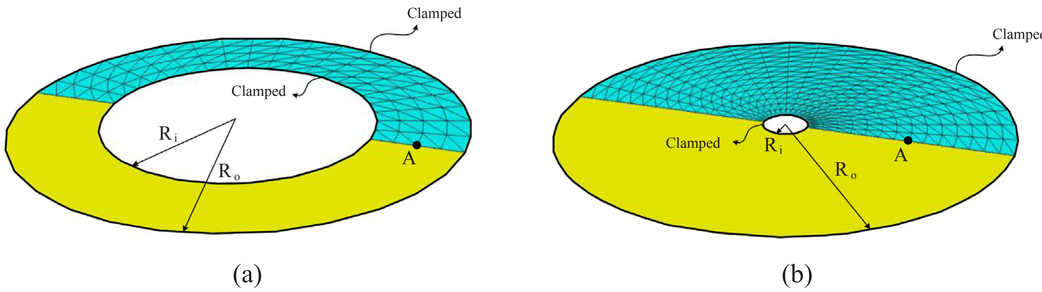

Fig. 6. Annular plate, (a) $\beta = 0.6$, (b) $\beta = 0.1$

Table 2
Comparison of the critical thermal load (ΔT_{cr}) with various geometric characterizations.

case (I)	β					
	0.1	0.2	0.3	0.4	0.5	0.6
Present study Fig. 7 (K)	223	298	377	501	725	1107
Ghiasian et al. [13] (K)	227	283	376	510	724	1109
case (II)	δ					
	0.01	0.015	0.02	0.025	0.03	0.035
Present study Fig. 7 (K)	80	179	319	503	717	967
Ghiasian et al. [13] (K)	84	190	332	514	729	981

The material properties are as follows:

Aluminium Oxide (Al_2O_3): $E_c = 380 \times 10^5\,\mathrm{N/cm^2}$,
$\alpha_c = 7.4 \times 10^{-6}\,\mathrm{K^{-1}}$, $\nu_c = 0.3$
Aluminium (Al) : $E_m = 70 \times 10^5\,\mathrm{N/cm^2}$,
$\alpha_m = 23 \times 10^{-6}\,\mathrm{K^{-1}}$, $\nu_m = 0.3$

Firstly, a temperature change of $\Delta T = 1000\,K$ is assumed to be applied. To trace the secondary equilibrium path, it is necessary to perturb the structure. It is done by applying two opposite outward diametrical point loads of 4000 N. The responses of the thermal buckling are plotted in Fig. 11(a). In second study, the conical shell is considered to be subjected to pressure load of $p = 10000\,\mathrm{N/cm^2}$. Obtained solutions are presented in terms of load-displacement curves in Fig. 11(b). Finally, the nonlinear behavior of current structure is investigated under the thermo-mechanical loading. The temperature field employed here is $\Delta T = 1000\,\mathrm{K}$ accompanying by a pressure load of $p = 10000\,\mathrm{N/cm^2}$.

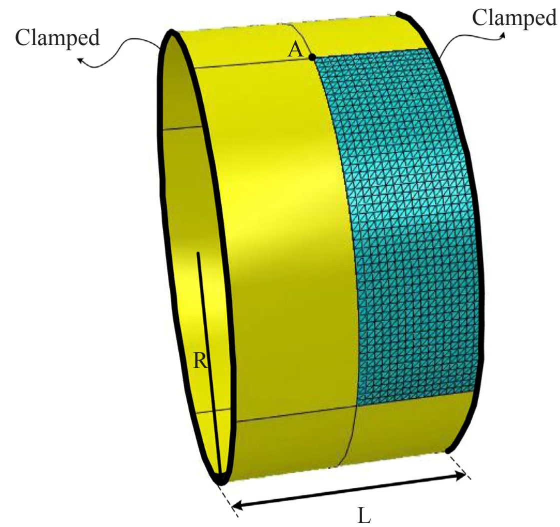

Fig. 8. Clamped cylindrical shell

Fig. 11(c) denotes the results due to the thermo-mechanical loading. Note that all the responses are obtained for the point A. It is worth mentioning that only one-fourth of the structure is modeled by $2 \times 16 \times 32$ triangular element, due to the shell symmetry. It is seen that the buckling temperature increases with decrease of *n*. In the thermal loading case, the structure displays a limit point, which is followed by a snap-through behavior. This unstable part gradually vanishes as the value of *n* raises.

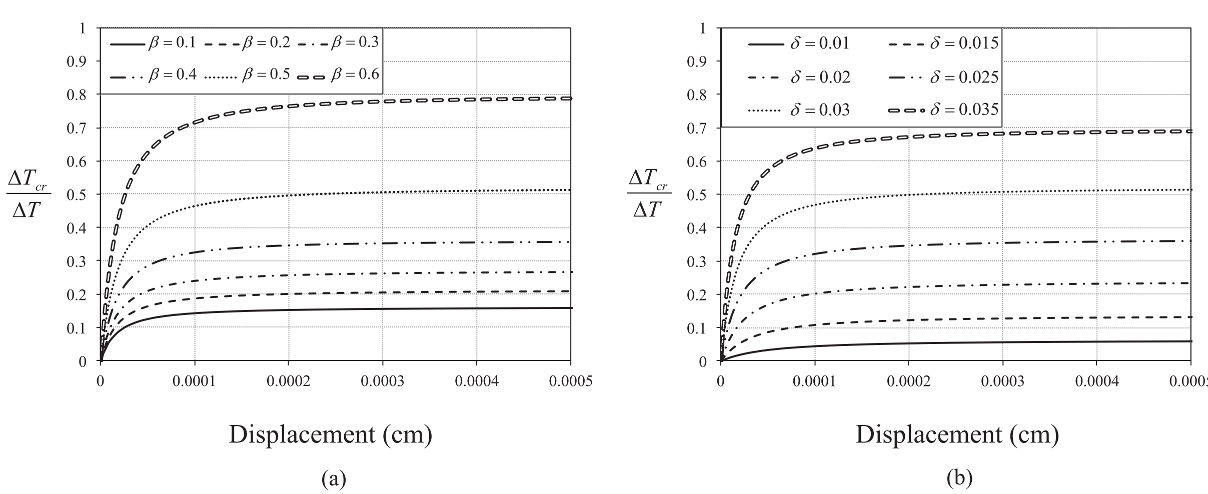

Fig. 7. Load-deflection curves of annular plate with various geometric data, (a) case(I), (b) case(II)

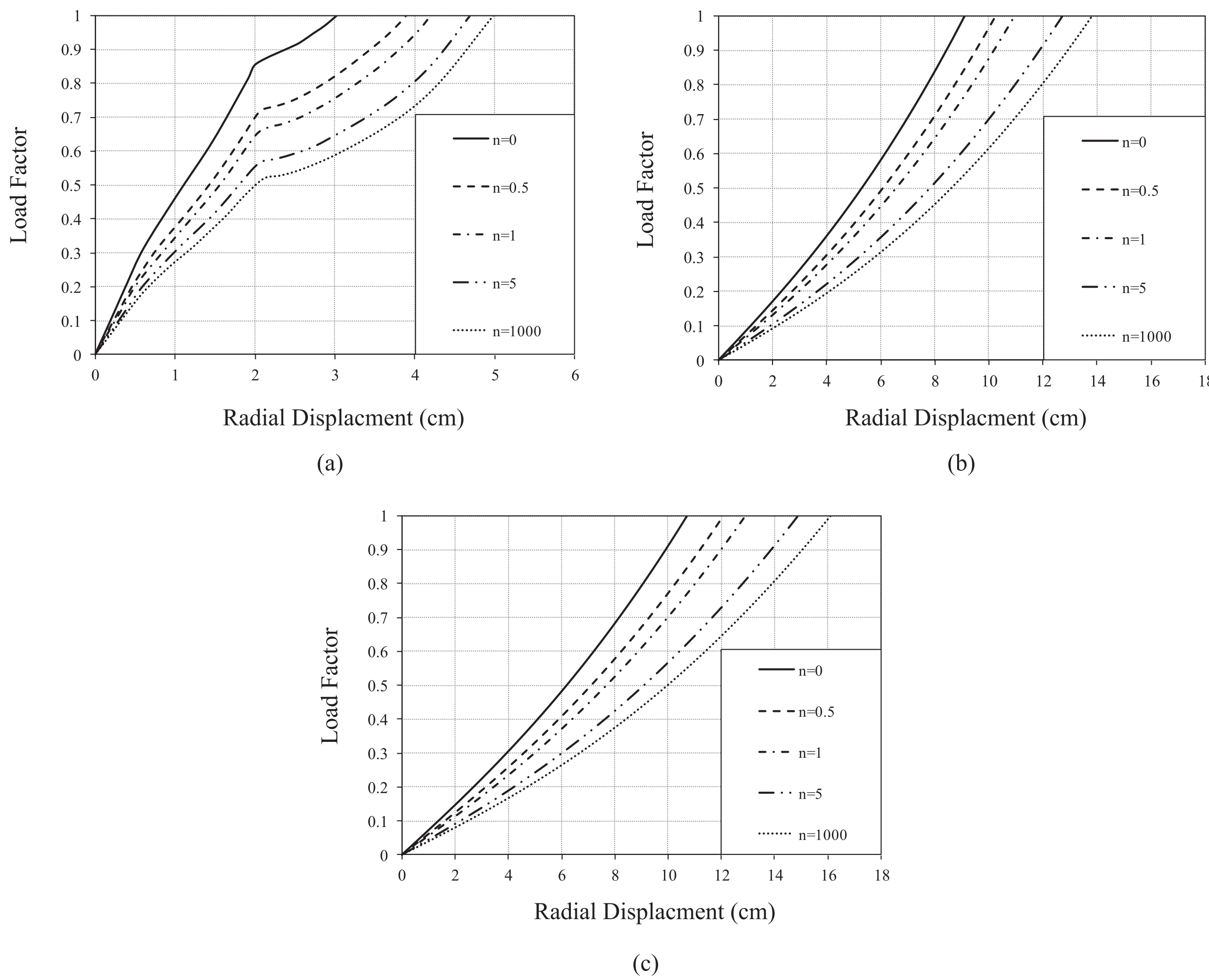

Fig. 9. Load-displacement curves of cylindrical shell at point A, (a) Thermal load, (b) Mechanical load, (c) Thermo-mechanical load

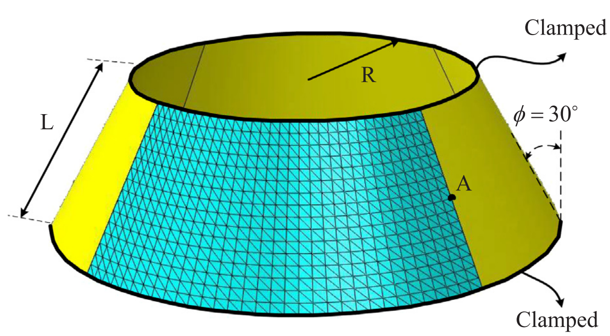

Fig. 10. Truncated conical shell

Table 3
Geometric characteristics of truncated conical shell.

Radius of large span R	*Radius of small span R*	*Length L*	*Thickness h*
150 cm	100 cm	100 cm	1 cm

9. Conclusions

Studies on nonlinear analysis of various and arbitrary FG shells under thermo-mechanical loading are limited in the available literature. In the cases with strong nonlinearity, the linear eigenvalue buckling analysis estimated much more or less the true buckling temperature values. To reach more exact predictions and fill the gap, the nonlinear FE based analysis of arbitrary FG shells subjected to thermo-mechanical loading was performed in this article. A second-order and six-noded isoparametric triangular shell element was developed for the general purposes. Each element's node had all six independent degrees of freedom in space. It should be mentioned that the material properties were expressed by Voigt's model. After performing extensive numerical studies, some new outcomes were found.

1. Pre-buckling (primary) path was almost linear, while the post-buckling (secondary) path had a nonlinear nature.
2. Additional disturbance load, like a geometric imperfection, led to reduction of the buckling temperature and vice versa.
3. In FG shallow cylindrical panel, reduction of shell thickness results in a more complex equilibrium path, including snap-through and snap-back responses.
4. The thermal buckling load of annular plate increases as the values of β and δgrows. This is owing to the fact that raising the values of δandβresults in stiffer structure.
5. In all numerical studies, it is observed that structure behaves stiffer as the volume fraction index n decreases.

Acknowledgements

It is acknowledged that all parts of these computations were performed on the High-Performance Computing (HPC) center of Ferdowsi University of Mashhad.

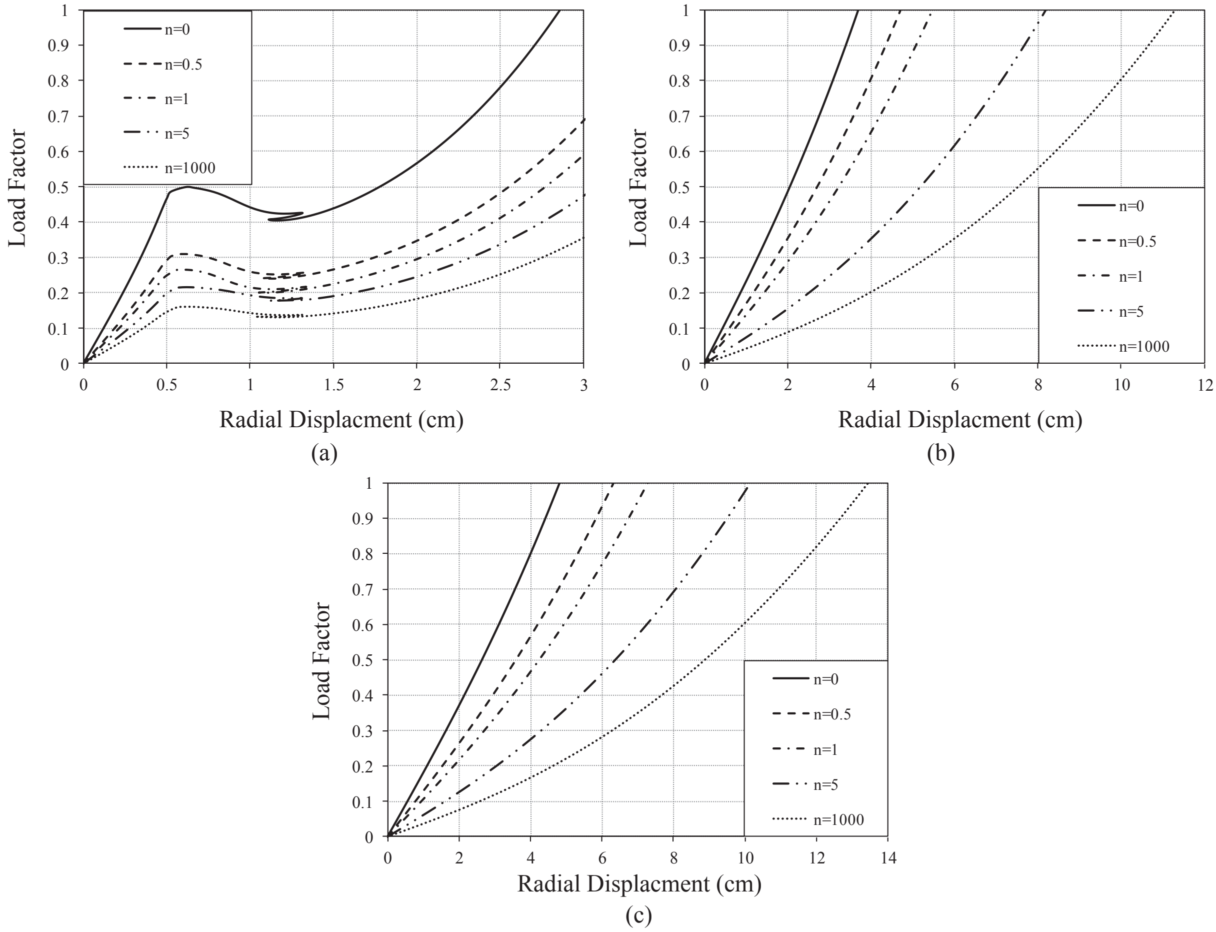

Fig. 11. Load-displacement curves of conical shell at point A, (a) Thermal load, (b) Mechanical load, (c) Thermo-mechanical load

Appendix A. Supplementary material

Supplementary data to this article can be found online at https://doi.org/10.1016/j.engstruct.2018.09.084.

References

[1] Birman V, Byrd LW. Modeling and analysis of functionally graded materials and structures. Appl Mech Rev 2007;60:195–215.
[2] Jha DK, Kant T, Singh RK. A critical review of recent research on functionally graded plates. Compos Struct 2013;96:833–49.
[3] Thai HT, Kim SE. A review of theories for the modeling and analysis of functionally graded plates and shells. Compos Struct 2015;128:70–86.
[4] Reddy JN, Chin CD. Thermomechanical analysis of functionally graded cylinders and plates. J Therm Stress 1998;21:593–626.
[5] Woo J, Meguid SA. Nonlinear analysis of functionally graded plates and shallow shells. Int J Solids Struct 2001;38:7409–21.
[6] Patel BP, Shukla KK, Nath Y. Nonlinear thermoelastic stability characteristics of cross-ply laminated oval cylindrical/conical shells. Finite Elem Anal Des 2006;42:1061–70.
[7] Hosseini Kordkheili SA, Naghdabadi R. Geometrically nonlinear thermoelastic analysis of functionally graded shells using finite element method. Int J Numer Meth Eng 2007;72:964–86.
[8] Shen HS. Thermal postbuckling of shear deformable FGM cylindrical shells with temperature-dependent properties. Mech Adv Mater Struct 2007;14:439–52.
[9] Huang H, Han Q. Nonlinear buckling and postbuckling of heated functionally graded cylindrical shells under combined axial compression and radial pressure. Int J Non-linear Mech 2009;44:209–18.
[10] Alijani F, Amabili M, Bakhtiari-Nejad F. Thermal effects on nonlinear vibrations of functionally graded doubly curved shells using higher order shear deformation theory. Compos Struct 2011;93:2541–53.
[11] Torabi J, Kiani Y, Eslami MR. Linear thermal buckling analysis of truncated hybrid FGM conical shells. Compos Part: B 2013;50:265–72.
[12] Shen HS, Wang H. Nonlinear bending of FGM cylindrical panels resting on elastic foundations in thermal environment. Eur J Mech A/Solids 2015;49:49–59.
[13] Ghiasian SE, Kiani Y, Sadighi M, Eslami MR. Thermal buckling of shear deformable temperature dependent circular/annular FGM plates. Int J Mech Sci 2014;81:137–48.
[14] Beheshti A, Ramezani S. Nonlinear finite element analysis of functionally graded structures by enhanced assumed strain shell elements. Appl Math Model 2015;39:3690–703.
[15] Kar VR, Panda SK. Thermoelastic analysis of functionally graded doubly curved shell panels using nonlinear finite element method. Compos Struct 2015;129:202–12.
[16] Kar VR, Mahapatra TR, Panda SK. Effects of different temperature load on thermal postbuckling behaviour of functionally graded shallow curved shell panels. Compos Struct 2017;160:1236–47.
[17] Frikha A, Dammak F. Geometrically non-linear static analysis of functionally graded material shells with a discrete double directors shell element. Comput Meth Appl Mech Eng 2017;315:1–24.
[18] Sofiyev AH, Kuruoğlu N. The stability of FGM truncated conical shells under combined axial and external mechanical loads in the framework of the shear deformation theory. Compos Part: B 2016;92:463–76.
[19] Moosaie A, Panahi-Kalus H. Thermal stresses in an incompressible FGM spherical shell with temperature-dependent material properties. Thin-walled Struct 2017;120:215–24.
[20] Rezaiee-Pajand M, Arabi E, Masoodi AR. A triangular shell element for geometrically nonlinear analysis. Acta Mech 2018;229:323–42.
[21] Rezaiee-Pajand M, Arabi E. A curved triangular element for nonlinear analysis of laminated shells. Compos Struct 2016;153:538–48.
[22] Li X, Du CC, Li YH. Parametric instability of a functionally graded cylindrical thin shell subjected to both axial disturbance and thermal environment. Thin-walled Struct 2018;123:25–35.
[23] Prakash T, Singha MK, Ganapathi M. Thermal postbuckling analysis of FGM skew plates. Eng Struct 2008;30:22–32.
[24] Abolghasemi S, Shaterzadeh AR, Rezaei R. Thermo-mechanical buckling analysis of functionally graded plates with an elliptic cutout. Aerosp Sci Technol 2014;39:250–9.
[25] Yu T, Yin S, Bui TQ, Liu C, Wattanasakulpong N. Buckling isogeometric analysis of functionally graded plates under combined thermal and mechanical loads. Compos Struct 2017;162:54–69.
[26] Lin Q, Chen F, Yin H. Experimental and theoretical investigation of the thermo-mechanical deformation of a functionally graded panel. Eng Struct 2017;138:17–26.

[27] Masoodi AR, Arabi E. Geometrically nonlinear thermomechanical analysis of shell-like structures. J Therm Stress 2018;41:37–53.
[28] Argyris J. An excursion into large rotations. Comput Meth Appl Mech Eng 1982;32:85–155.
[29] Sansour C, Bufler H. An exact finite rotation shell theory, its mixed variational formulation and its finite element implementation. Int J Numer Meth Eng 1992;34:73–115.
[30] Campello EMB, Pimenta PM, Wriggers P. A triangular finite shell element based on a fully nonlinear shell formulation. Comput Mech 2003;31:505–18.
[31] Pimenta PM, Campello EMB. Shell curvature as an initial deformation: a geometrically exact finite element approach. Int J Numer Meth Eng 2009;78:1094–112.
[32] Simo JC, Hughes TJR. Computational inelasticity. New York: Springer; 1998.
[33] Chróścielewski J, Makowski J, Stumpf H. Genuinely resultant shell finite elements accounting for geometric and material non-linearity. Int J Numer Meth Eng 1992;35:63–94.
[34] Sansour C, Berdnarczyk H. The cosserat surface as a shell model, theory and finite element formulation. Comput Meth Appl Mech Eng 1995;120:1–32.
[35] Arciniega RA, Reddy JN. Tensor-based finite element formulation for geometrically nonlinear analysis of shell structures. Comput Meth Appl Mech Eng 2007;196:1048–73.